Available online at www.sciencedirect.com
SCIENCE DIRECT®

Journal of the European Ceramic Society 24 (2004) 3209–3218

www.elsevier.com/locate/jeurceramsoc

# Permeability of ceramic foams to compressible and incompressible flow

E.A. Moreira[a], M.D.M. Innocentini[b], J.R. Coury[a,*]

[a]Department of Chemical Engineering, Universidade Federal de São Carlos, Rod.Washington Luiz, km 235, CEP:13565-905, São Carlos, SP, Brazil
[b]Department of Materials Engineering, Universidade Federal de São Carlos, Rod.Washington Luiz, km 235, CEP:13565-905, São Carlos, SP, Brazil

Received 15 July 2003; received in revised form 27 October 2003; accepted 3 November 2003

**Abstract**

Ceramic foams constitute a new structural material characterized by a high porosity and high superficial area, formed by mega-pores interconnected by filaments. This results in a structure with low resistance to fluid flow, and to their use as filter. This work investigates the influence of several structural parameters, such as porosity, tortuosity, surface area and pore diameter, in predicting the permeability of ceramic foams. Foams with different pore densities were used as porous media. The permeability was measured utilizing air and water as flowing fluids, the former taken as an ideal gas and the latter as incompressible. No existing correlation was able to predict the permeability in the whole range studied. An Ergun-type correlation was fitted to the data, and represented very well the permeability of the media for all the foams, flowing fluids and operational range studied. Pore diameter was the structural parameter that best represented the media.


*Keywords:* Foams; Mechanical properties; Membranes; Non-destructive evaluation; Permeability; SiC–$Al_2O_3$; Structural applications

## 1. Introduction

Ceramic bodies present, in general, good mechanical, chemical and thermal resistance,[1] and, as porous ceramic materials, are widely utilized as filters for hot gas cleaning,[2,3] in the purification of liquid metals,[4] as acoustic absorbers, bioreactors,[5] heat exchangers, etc.

Amongst the ceramic media, the cellular ceramics are becoming an interesting alternative as structural components in the solid–fluid separation technology in the last decades.[6,7] The cellular ceramics consist of several open cells arranged in honeycomb or foam-like structures. These structures present a high number of interconnected pores, which results in low resistance to the flow of fluids. They also have low density and controlled pore size and, with the appropriate combination of ceramic materials and processing techniques, also show very good performance in all aspects regarding ceramic materials.

In general, the mechanical behavior and the structural characterization of the ceramic foams are relatively well explored in the literature, but the same cannot be said of the permeability, one of the main filtration parameters.

Most of the models used in the determination of the permeability in these media are derived from correlations originally developed for granular beds, and this often leads to gross deviations. Due to the singular characteristics of the foams, one of the main difficulties in the derivation of such models is in identifying structural characteristics that represent the cellular media realistically.

This work examines the effect of a number of structural parameters, such as the effective porosity (i.e., the porosity that effectively contributes to the fluid flow), the tortuosity, the specific surface area and the pore diameter, in the prediction of the bed permeability based on existing models found in the literature. Some of the models were applied as derived for granular beds and others have already been adapted to cellular media.

The effective porosity was obtained from the stimulus-response method (time of residence) and the pore diameter and surface area were obtained by image analysis. The latter was also obtained by the use of

* Corresponding author. Tel.: +55-16-260-8264; fax: +55-16-260-8266.
*E-mail address:* jcoury@power.ufscar.br (J.R. Coury).

0955-2219/$ - see front matter © 2003 Elsevier Ltd. All rights reserved.
doi:10.1016/j.jeurceramsoc.2003.11.014

**Nomenclature**

| | |
|---|---|
| $a_{vs}$ | specific surface area [$L^{-1}$] |
| $C_i$ | tracer concentration at the bed exit at time $t_i$ [$ML^{-3}$] |
| $D$ | bed diameter [L] |
| $d_p$ | particle diameter [L] |
| $d_{pore}$ | pore diameter [L] |
| $F$ | formation factor [−] |
| $k_1$ | Darcyan permeability coefficient [$L^2$] |
| $k_2$ | non-Darcyan permeability coefficient [L] |
| $L$ | bed thickness [L] |
| $L_e$ | real (tortuous) length traveled by the flowing fluid [L] |
| $P_i$ | pressure at bed entrance [$ML^{-1}\ t^{-2}$] |
| $P_o$ | pressure at bed exit [$ML^{-1}\ t^{-2}$] |
| $Q$ | volumetric flow rate [$L^3\ t^{-1}$] |
| Re | bed Reynolds number ($\rho v D/\mu$) [−] |
| $Re_{pore}$ | pore Reynolds number ($\rho v d_{pore}/\mu$) [−] |
| $t$ | time of flow through the volume without the porous medium [t] |
| $t^*$ | time of flow through the volume with the porous medium [t] |
| $\bar{t}$ | average residence time [t] |
| $v$ | volumetric flow rate per unit bed cross-section [$Lt^{-1}$] |
| $V_F$ | volume of the open voids [$L^3$] |
| $V_F^*$ | volume occupied by the flowing fluid [$L^3$] |
| $V_T$ | total bed volume [$L^3$] |
| $\Delta P$ | pressure drop [$ML^{-1}\ t^{-2}$] |

*Greek letters*

| | |
|---|---|
| $\alpha$ | empirical parameter of Eq. (7) |
| $\beta$ | empirical parameter of Eq. (8) |
| $\delta_c$ | electrical resistivity of the conductive solution [H] |
| $\delta_m$ | electrical resistivity of the medium saturated with the solution [H] |
| $\varepsilon$ | bed total porosity [−] |
| $\varepsilon^*$ | effective porosity [−] |
| $\rho$ | fluid density [$ML^{-3}$] |
| $\rho_b$ | bed apparent density [$ML^{-3}$] |
| $\rho_s$ | solid density [$ML^{-3}$] |
| $\mu$ | fluid viscosity [$ML^{-1}\ t^{-1}$] |
| $\tau$ | tortuosity [−] |

correlations proposed by Richardson et al. and by Gibson and Ashby.[8,9] The tortuosity was obtained by measuring the electric resistivity of the medium. The utilized ceramic foams were made of SiC–$Al_2O_3$, and have linear pore densities of 8, 20 and 45 pores per inch (ppi). The permeability was measured utilizing air and water as flowing fluids, the former taken as an ideal gas and the latter as incompressible.

## 2. Permeability of porous media

The permeability of a fluid when flowing through a porous medium is usually quantified by the Forchheimer equation, described as:

$$\frac{\Delta P}{L} = \frac{\mu}{k_1}\ v + \frac{\rho}{k_2}\ v^2 \tag{1}$$

where $\Delta P$ is the pressure drop, $L$ is the medium thickness, $\rho$ and $\mu$ are the viscosity and the density of the fluid, respectively, and $v$ is the volumetric flow rate per unit of cross-sectional area of the flowing fluid. The pressure drop $\Delta P$ is given by Eq. (1a) in the case of incompressible fluids and by Eq. (1b) for compressible fluids (ideal gases).

$$\Delta P = P_i - P_o \tag{1a}$$

$$\Delta P = \frac{P_i^2 - P_o^2}{2P_o} \tag{1b}$$

where $P_i$ and $P_o$ are the absolute pressures at the bed entrance and exit, respectively. $P_i$ is the reference pressure for the density and viscosity of the flowing fluid.

The parameters $k_1$ and $k_2$ are usually referred as the Darcyan and non-Darcyan permeability parameters, respectively. These parameters are assumed to incorporate the structural properties of the medium, and to be a function of the bed characteristics only.[10]

Of the correlations that incorporate characteristics of the porous medium, the one proposed by Ergun[11] is the more used, and was derived from the flow through granular beds. This correlation has the same general form as that of Eq. (1), and is expressed as:

$$\frac{\Delta P}{L} = 150\frac{(1-\varepsilon)^2}{\varepsilon^3}\frac{\mu v}{d_p^2} + 1.75\frac{(1-\varepsilon)}{\varepsilon^3}\frac{\rho v^2}{d_p} \tag{2}$$

where $\varepsilon$ is the bed porosity and $d_p$ it is the median surface-volume diameter of the particles that form the granular bed.

Following the same idea and working with several forms of spherical and non-spherical particles, a number of researchers have proposed different values for the numerical constants in Eq. (2), but no relevant improvement was achieved. A thorough review on this subject is presented by Macdonald et al.[12]

For the cellular media, there are few proposed correlations, as the one proposed by DuPlessis et al.[13] They consider the cellular medium formed by cubic unit cells, leading to the following correlations:

$$\frac{\Delta P}{L} = \frac{36\tau(\tau-1)}{\varepsilon^2}\frac{\mu v}{d_{\text{pore}}^2} + \frac{2.05\tau(\tau-1)}{\varepsilon^2(3-\tau)}\frac{\rho v^2}{d_{\text{pore}}} \quad (3)$$

where $\tau$ is the medium tortuosity and $d_{\text{pore}}$ is the pore diameter.

A more recent correlation was proposed by Richardson et al.,[8] in which the authors, based on the work of Gibson and Ashby,[9] consider that the cellular medium is formed by uniform tri-dimensional cells. For these authors, the expression for $\Delta P/L$ in SI units is given by:

$$\frac{\Delta P}{L} = \frac{\alpha a_{\text{vs}}^2(1-\varepsilon)^2}{\varepsilon^3}\mu v + \frac{\beta a_{\text{vs}}(1-\varepsilon)}{\varepsilon^3}\rho v^2 \quad (4)$$

where the parameters $\alpha$ and $\beta$ are given by:

$$\alpha = 973 d_{\text{pore}}^{0.743}(1-\varepsilon)^{-0.0982} \quad (5)$$

$$\beta = 368 d_{\text{pore}}^{-0.7523}(1-\varepsilon)^{0.07158} \quad (6)$$

According to the authors, the specific surface area can be calculated by:

$$a_{\text{vs}} = \frac{12.979\left[1-0.971(1-\varepsilon)^{0.5}\right]}{d_{\text{pore}}(1-\varepsilon)^{0.5}}. \quad (7)$$

While for granular media the particle diameter has its dependence correctly quantified by Ergun,[11] it is not clear the role of the pore diameter in a cellular structure. Another subject to be considered is the role of total porosity and of the effective porosity (i.e., the porosity that contributes for the flow of the fluid inside the porous medium) in the permeability parameters. These parameters, as well as the bed tortuosity and specific surface area were measured and used in the respective correlations.

## 3. Materials and methods

### 3.1. The cellular media

The ceramic foams utilized in this work were manufactured utilizing the replica technique, where a polymeric foam has its filaments coated with a ceramic suspension. A subsequent thermal treatment removes the organic material, remaining the ceramic material in the substratum. This method allows the production of regular structures once good quality organic foams are used as matrixes. The foams are specified commercially by the count of pores per linear inch (ppi) and attention must be taken to their uniformity.

Ceramic samples made from SiC–$Al_2O_3$ powders, and the polymeric foams used as matrixes were polyurethane foams with highly uniform pores. The foams were soaked with the ceramic mix, followed by calcination. Details are given in Moreira et al.[14] Also, a fixed bed of glass spheres, with diameter of 2.95 mm, was used for comparison. All media were made at the DEQ and DEMa laboratories, at UFSCar. Fig. 1 illustrates the cellular foams utilized, with pore densities of 8, 20 and 45 pores per inch (ppi).

### 3.2. Permeability measurements

The general view of the equipments used for permeability measurements of the ceramic foams are illustrated in Fig. 2. The fluids used in the experiments were water (Fig. 2a) and air (Fig. 2b) in ambient temperature. For the water permeability measurements, the mass flow rate was obtained by weighing water that flowed through the sample in a given period of time. For the air permeability, the mass flow rate was calculated from the volumetric flow, measured by a rotameter, and corrected for the temperature and pressure. In both cases, the pressure drop was measured utilizing a micro-

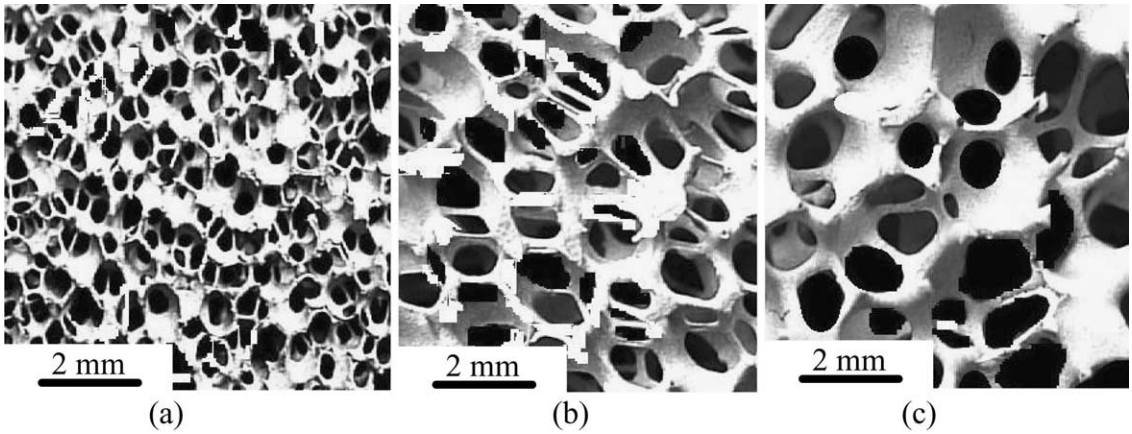


Fig. 1. Photographs of the utilized ceramic foams with: (a) 45 ppi; (b) 20 ppi; (c) 8 ppi.

manometer (Furness FC016). The tested samples were 8, 20 and 45 ppi ceramic foams disks with diameter of 7.5 cm and thicknesses of 3.0, 2.9 and 1.4 cm, respectively. The experiments were made in triplicates and the pressure drop was plotted as function of the fluid superficial velocity, $v$. Eq. (1) was used to calculate the experimental permeability constants $k_1$ and $k_2$.

### 3.3. Total and effective porosity

The total porosity of a porous bed is defined as:

$$\varepsilon = \frac{\text{volume of the open voids}}{\text{total bed volume}} = \frac{V_F}{V_T} \tag{8}$$

But not all the fluid that fills the voids within a porous medium flows when a pressure difference is applied. Part of this fluid remains stagnated and do not contribute for the fluid flow rate. The effective porosity, i.e. the one that contributes for the flow, can be defined as:

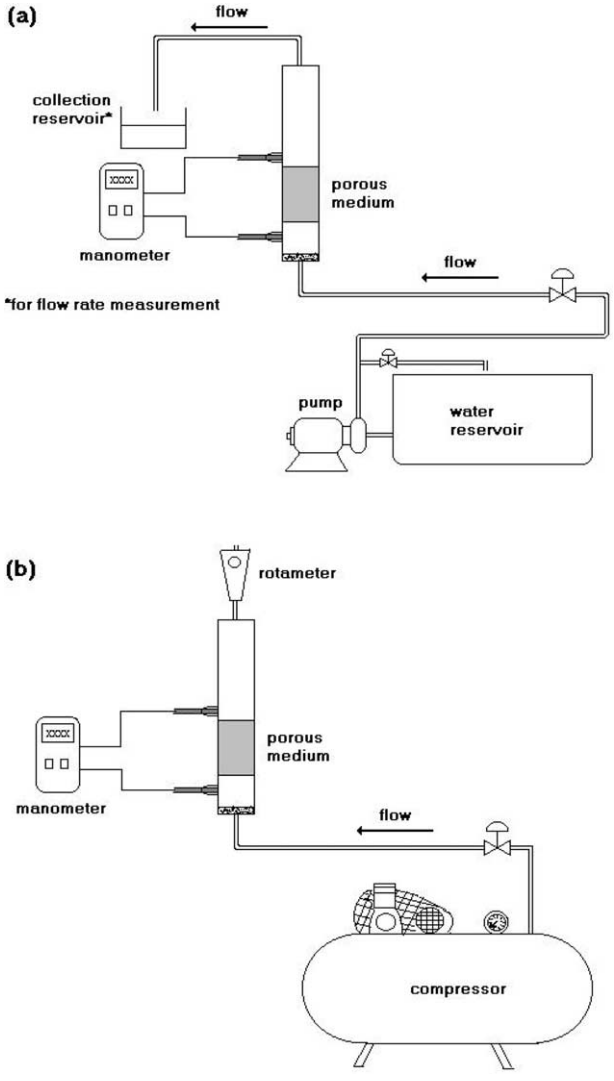


Fig. 2. General view of the equipments for the permeability measurements of (a) water and (b) air.

$$\varepsilon^* = \frac{\text{vol. occupied by the flowing fluid}}{\text{total bed volume}} = \frac{V_F^*}{V_T} \tag{9}$$

If a porous bed is fed with a fluid with a volumetric flow rate $Q$, then:

$$Q = \frac{\text{volume of flowing fluid}}{\text{time}} = \frac{V_F^*}{t^*} \tag{10}$$

where $t^*$ is the time of flow of the fluid through the medium.

For the bed without the porous medium, with the same total volume, the flow rate is given by:

$$Q = \frac{\text{total volume}}{\text{time}} = \frac{V_T}{t} \tag{11}$$

For the same flow rate, the effective porosity [Eq. (9)] can be calculated by equating Eqs. (10) and (11). The result is:

$$\varepsilon^* = \frac{t^*}{t} \tag{12}$$

Therefore $\varepsilon^*$, the effective porosity, can be obtained from the ratio between the residence time in a given volume, with and without porous medium, respectively, for the same flow rate $Q$.

The total porosity of the media can be measured utilizing Eq. 13:

$$\varepsilon = 1 - \frac{\rho_b}{\rho_s} \tag{13}$$

where $\rho_b$ is the apparent density of the sample (mass/total sample volume) and $\rho_s$ is the solid phase density, measured here with a Micromeritics Helium Picnometer.

### 3.4. The residence time estimate

The average residence time can be obtained from the residence time distribution (RTD), using the stimulus-response technique. In this technique, a non-reactive tracer pulse is injected into the flowing fluid as it enters the porous bed and the concentration of this tracer is measured in the exit, as function of time.

In this case, Levenspiel[15] defined the average residence time as:

$$\bar{t} = \frac{\int_0^\infty tCdt}{\int_0^\infty Cdt} = \frac{\sum t_i C_i \Delta t_i}{\sum C_i \Delta t_i} \tag{14}$$

in which $\bar{t}$ (assumed here as $t^*$) is the average residence time and $C_i$ is the concentration of the tracer in the exit of the porous bed at the time $t_i$.

For determination of the residence time, a system for data acquisition was built, that consisted of a duct containing the porous medium. A pulse of a previously calibrated NaCl solution was injected before the

medium, and a probe (CBL 2, Texas Instruments), was placed after it. The probe was connected to a TI-89 calculator (Texas Instruments), wich measured and stored the concentration of the tracer as a function of time. Fig. 3 illustrates the rig utilized for the residence time measurements.

### 3.5. Tortuosity

Sheidegger[16] defined the tortuosity as the ratio between the real length that the fluid travels inside of a medium ($L_e$) and the thickness of the medium ($L$). The author suggests that it can be obtained by measuring of the formation factor $F$, which is given by the electrical resistivity of the porous medium completely saturated with a conductive solution ($\delta_m$) divided by resistivity of the solution alone ($\delta_s$). Therefore:

$$F = \frac{\delta_m}{\delta_s} \tag{15}$$

and the tortuosity is given by:

$$\tau = \varepsilon F \tag{16}$$

The tortuosity tests were accomplished in the equipment shown in Fig. 4. For these experiments, Ag/AgCl reference electrodes were used in Luggin capillary filled out with a 0.3 mol KCl solution. These electrodes were connected to the test chamber and to a voltmeter to measure the potential difference. In the test chamber, a 0.1 mol $H_2SO_4$ solution was used as test solution. The current was supplied by a source that varied from 0 to 15 mA. For the experiments, the largest current value utilized was of 8mA, so that hydrogen formation could be avoided.

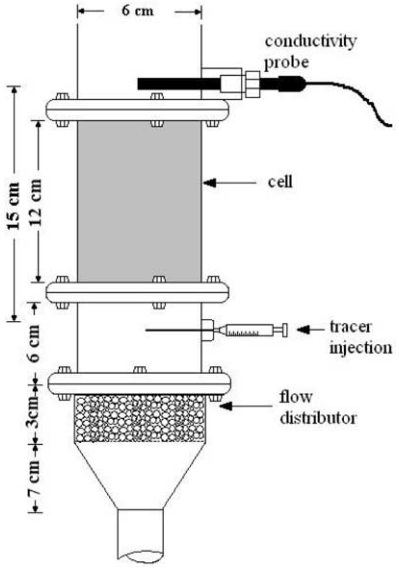


Fig. 3. The rig utilized for the residence time measurements.

The experimental procedure consisted of measuring the potential difference for each value of applied current, for the test chamber filled out with the solution of $H_2SO_4$ alone and also for the chamber comprising the porous medium and the solution. The measured potential differences were plotted as a function of the current, resulting in straight lines, whose angular coefficients constitute the resistivities of the solution and of the medium, respectively. The tortuosity was calculated utilizing Eq. (16). For both porosity and tortuosity experiments samples consisted of 8, 20 e 45 ppi ceramic foams disks with diameter of 7.5 cm and thicknesses of 11.72, 11.95 and 4.4 cm, respectively.

### 3.6. Pore diameter and specific surface area

The diameter of the pores for each sample was obtained by image analysis, using the software Image Pro-Plus.

The specific surface area was obtained from measuring (by image analysis) the perimeter of the solid phase of a cross section of the foam and multiplying it by the length $L_e$ of the tortuous path, obtained from the tortuosity measurements.

## 4. Results and discussion

### 4.1. Experimental measurements of the structural parameters

Table 1 lists the structural parameters measured. The pore diameter decreased with the increase in the linear pore density, ppi, as expected. Less obvious, the bed total porosity decreased with the increase in ppi, probably due to pore clogging during foam formation, likely to occur more easily in smaller pores. This is confirmed by the tortuosity and by the specific surface area results, as both increase with ppi: the more clogged the medium

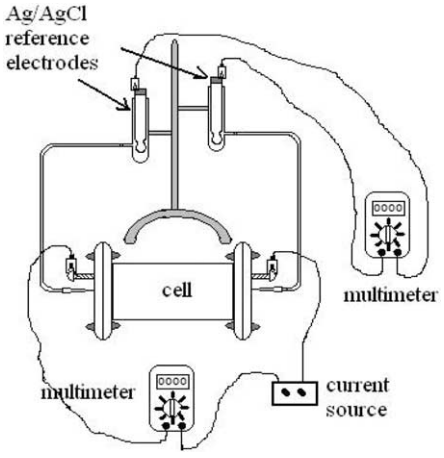


Fig. 4. Scheme of the equipment for the tortuosity measurements.

the more tortuous the fluid path and the higher the total wall surface. The tortuosity values are similar to reported values from the literature.[17] The measured specific surface areas are close to the ones predicted by Eq. (7).

Typical curves obtained from the equipment utilized for residence time measurement are shown in Fig. 5, were the tracer concentration at the bed exit is plotted as a function of time, for flow through a volume occupied by the 20 ppi foam medium (Fig. 5a) and for flow through the same volume with no medium (Fig. 5b). The different times for the concentration peaks were used for calculating the effective porosities utilizing Eq. (12).

Table 1
Measured pore diameters, porosities, tortuosities and specific surface areas

| Foam | $d_{pore}$ (mm) | Porosity | | Tortuosity | | Specific surface area | |
|---|---|---|---|---|---|---|---|
| | | $\varepsilon$ | $\varepsilon^{*a}$ | $\tau$ | $\tau^{*b}$ | $a_{vs}$ ($m^2/m^3$) | $a^{*b}_{vs}$ ($m^2/m^3$) |
| 8 ppi | 2.30 | 0.94 | 0.74/0.77 | 1.68 | 1.38 | $1.83\times10^4$ | $0.63\times10^4$ |
| 20 ppi | 0.80 | 0.88 | 0.71/0.73 | 1.71 | 1.42 | $1.92\times10^4$ | $0.71\times10^4$ |
| 45 ppi | 0.36 | 0.76 | 0.50/0.62 | 1.84 | 1.50 | $2.34\times10^4$ | $1.20\times10^4$ |
| gb[c] | 2.95 | 0.36 | 0.37/– | | | | |

[a] The two values reported refer to Q = 0.4 and 2.0 l/min, respectively.
[b] The symbol * refers to parameter calculated utilizing the effective porosity $\varepsilon^*$ for $q = 2$ l/min.
[c] Glass beads.

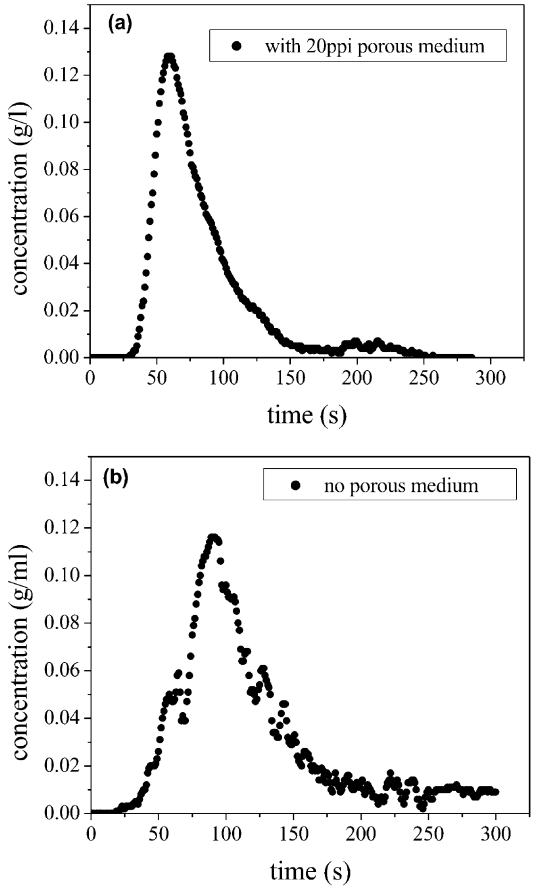


Fig. 5. Typical results from the residence time tests: tracer concentration at the bed exit as a function of time for (a) flow through the 20 ppi medium and (b) flow through the same volume with no medium. Data refer to a flow rate of 2 L/min.

Table 1 shows that the foam effective porosities are somewhat smaller than their total porosities, indicating that an appreciable amount of fluid remains stagnated (or recirculates locally) within the bed. These tests were made with two fluid flow rates (0.4 and 2 l/min). It is worth noting that the stagnated regions decrease as the flow rate increases.

As expected, these smaller values obtained for the effective porosities reflected accordingly in the effective tortuosities and specific surface areas, respectively, also shown in Table 1. The effective surface area can be understood as the interface between the flowing and the stagnated fluid.

### 4.2. The permeability measurements

Fig. 6 shows the permeability curves for the foams, utilizing air (Fig. 6a) and water (Fig. 6b) as flowing fluids. These tests were made in triplicate and the average and deviations are shown, indicating the good

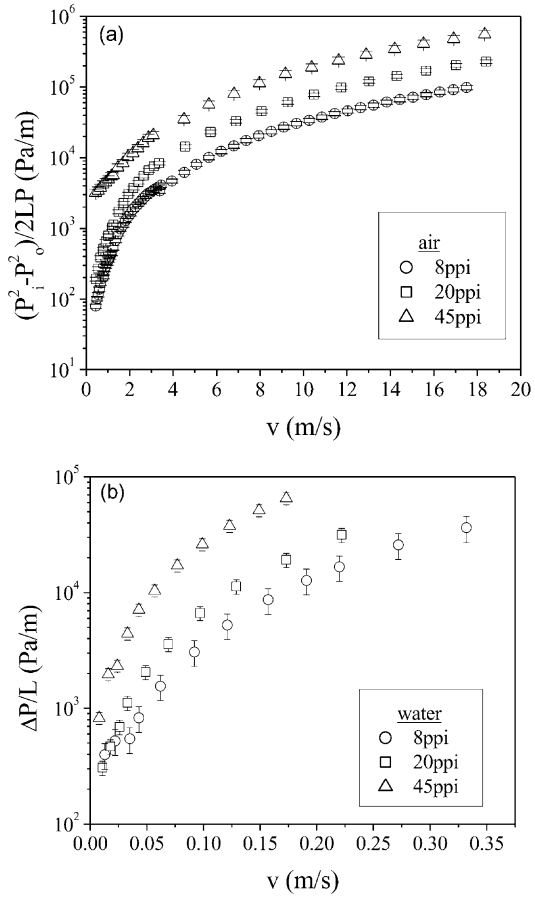


Fig. 6. The permeability tests performed with (a) air and (b) water.

reproducibility of the procedure. A wide range of bed Reynolds number, Re, was covered, that varied between $1\times10^2$ and $6.5\times10^4$ for air and $5\times10^2$ and $2.5\times10^4$ for water.

### 4.3. Comparison with correlations from the literature

Fig. 7 shows the permeability curve of air through a fixed bed of glass beads, utilizing the same equipment as for the foams. The results are very well represented by the classical Ergun equation, demonstrating the reliability of the apparatus.

Fig. 8 shows the comparison of the results with the theoretical correlations from the literature. In these curves, all the structural parameters utilized (porosity, tortuosity, specific surface area) were based on the foams total porosity. The left column refers to the air flow for the three foams investigated (Fig. 8a, 8c and 8e for 8, 20 and 45 ppi, respectively). The right column refers to water flow for the same foams (Figs. 8b, 8d and 8f for 8, 20 and 45 ppi, respectively). Four theoretical curves are plotted in all Figures: (i) the Ergun[11] correlation [Eq. (2)] replacing the particle diameter, $d_p$, by the pore diameter, $d_{pore}$, as suggested by Philipse and Schram;[18] (ii) the DuPlessis et al. correlation[13] (Eq. 3); (iii) the Richardson et al. correlation[8] [Eq. (4)], with $a_{vs}$ calculated by Eq. (7); and (iv) the Richardson et al. correlation[8] [Eq. (4)], with the experimental $a_{vs}$ measured here.

The comparison reveals that all theoretical predictions increase with increasing ppi. The general shape of all predictions curves was similar to the experimental points, but they did not give accurate predictions of the bed pressure drop. In the case of air, the predictions grow from an underestimate of the pressure drop for 8ppi [all but Eq. (3)] to an overestimate for 45 ppi. For water also, the estimates increase with ppi, and the pressure drop prediction is similar to that of the air flow. Of the four correlations tested, the Richardson et al. equation[8] [Eq. (4)] utilizing the experimental value of $a_{vs}$ was the one that exhibited smaller deviations as can be seen in Table 2: the deviations varied between 47 and 57%, which are fairly high.

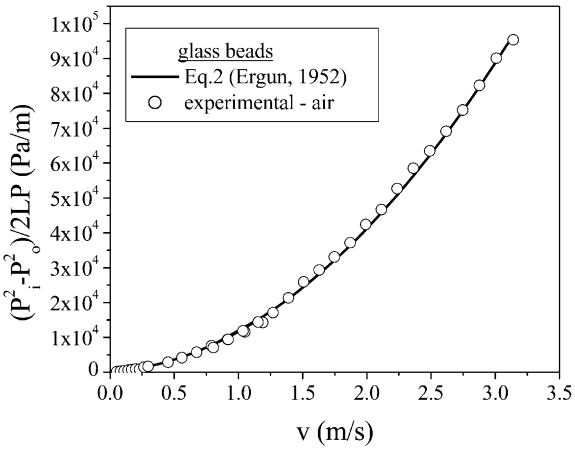


Fig. 7. Comparison between the experimental data and the curve predicted by the Ergun correlation [Eq. (2)], for a fixed bed of glass beads.

Fig. 9 shows the equivalent results of Fig. 8 for the structural parameters (porosity, tortuosity, specific surface area) based on the foams *effective* porosity. The results reveal that the predictions based on the effective parameters tended to lessen the scatter between the theoretical curves, when compared to the correspondent ones shown above. In these results the pressure drop was overestimated in all cases, but the tendency of increasing the overestimate with increasing ppi remains. Again here, the Richardson et al. equation[8] [Eq. (4)] utilizing the experimental value of $a_{vs}$ was the one that exhibited smaller deviations as can be seen in Table 2: the deviations varied between 56 and 109%, still very high and scattered.

In all, no correlation was able to predict the pressure drop, in the whole range of foams and fluids studied, and large deviations (as high as 654%) can be observed in Table 2.

Table 2
Maximum deviations for the correlations tested

| | Maximum deviation δ (%)[a] | | | | | |
|---|---|---|---|---|---|---|
| | ε | | | ε* | | |
| Correlation | 8 ppi | 20 ppi | 45 ppi | 8 ppi | 20 ppi | 45 ppi |
| Ergun (1952) [Eq. (2)] | 87 | 47 | 60 | 31 | 180 | 482 |
| Du Plessis et. al. (1994) [Eq. (3)] | 201 | 471 | 654 | 71 | 254 | 292 |
| Richardson et. al. (2000) [Eqs. (4) and (7)] | 54 | 150 | 247 | 110 | 415 | 484 |
| Richardson et. al. (2000) [Eqs. (4) with exp. $A_{vs}$] | 57 | 50 | 47 | 109 | 56 | 90 |
| Proposed correlation [Eq. (17)] | 9 | 12 | 12 | – | – | – |

[a] $\delta = \frac{1}{n}\sum_1^n \left|\frac{(y_{ex}-y_{cal})}{y_{ex}}\right| \times 100$; where $y_{ex}$ and $y_{cal}$ are the experimental and calculated values.

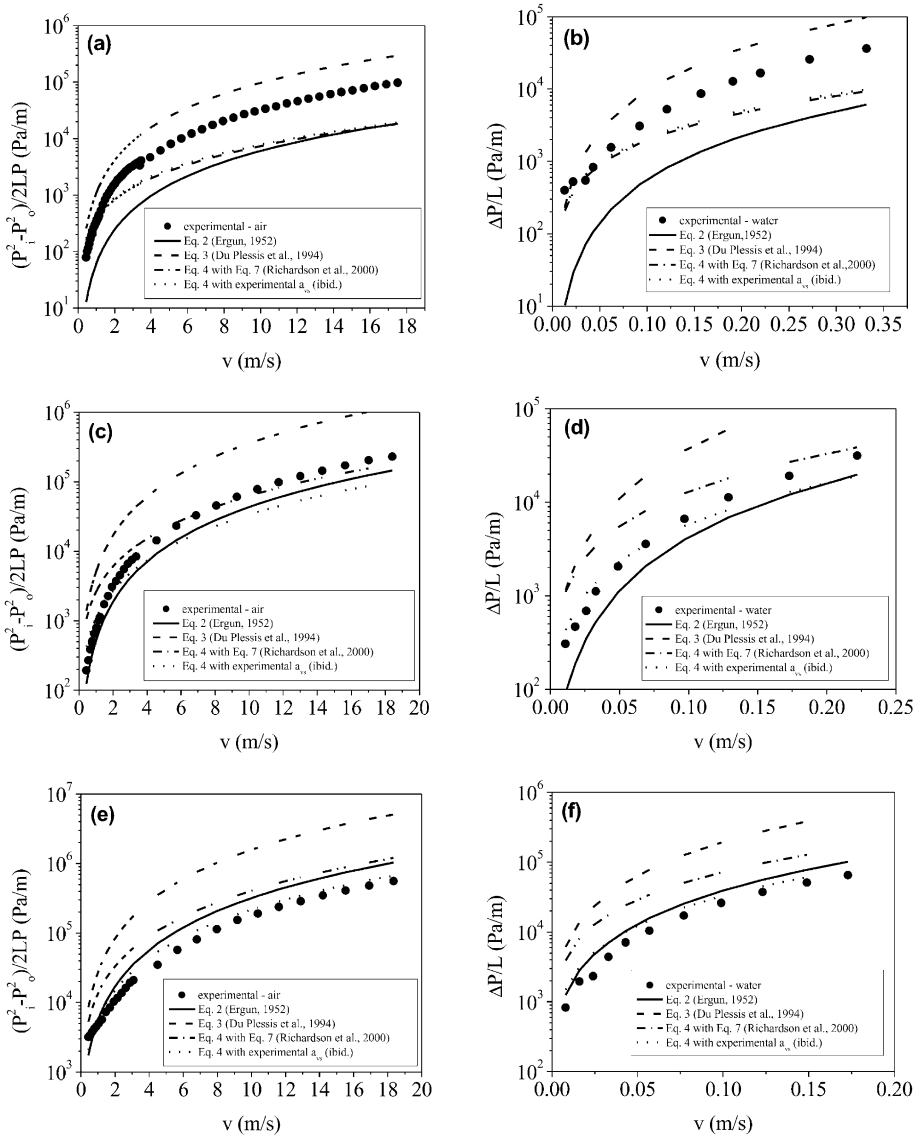


Fig. 8. Comparison between the experimental data and the curves predicted by models from the literature, utilizing the total porosity, tortuosity and specific surface area, for (a) 8 ppi, air; (b) 8 ppi, water; (c) 20 ppi, air; (d) 20 ppi, water; (e) 45 ppi, air; (f) 45 ppi, water.

### 4.4. The proposed correlation

As no single correlation covered the whole range studied, a multi-parameter fit of the experimental results was carried out. The Ergun equation was taken as a departing point, and numerous combinations were tested. The structural parameter $d_p$ (as the foams have no particle diameter) was replaced by other structural parameters ($a_{vs}$, $\tau$, $d_{pore}$), the two porosities ($\varepsilon$,$\varepsilon^*$) were used, and the numerical constants (150 and 1.75) were replaced by numerical values obtained from the fit. The best fit obtained was that utilizing the pore diameter, $d_{pore}$, and the total porosity, $\epsilon$, as structural parameters. The final correlation, for SI units, has the following form:

$$\frac{\Delta P}{L} = \frac{\mu v}{k_1} + \frac{\rho v^2}{k_2} \tag{17}$$

where $k_1$ and $k_2$ are given respectively by:

$$k_1 = \frac{\varepsilon^3 d_{pore}^{0.264}}{1.36 \times 10^8 (1-\varepsilon)^2} \tag{18}$$

$$k_2 = \frac{\varepsilon^3 d_{pore}^{-0.24}}{1.8 \times 10^4 (1-\varepsilon)} \tag{19}$$

These correlations are valid for $0.6 < Re_{pore} < 2.55 \times 10^3$ (water) and $0.36 < Re_{pore} < 805$ (air).

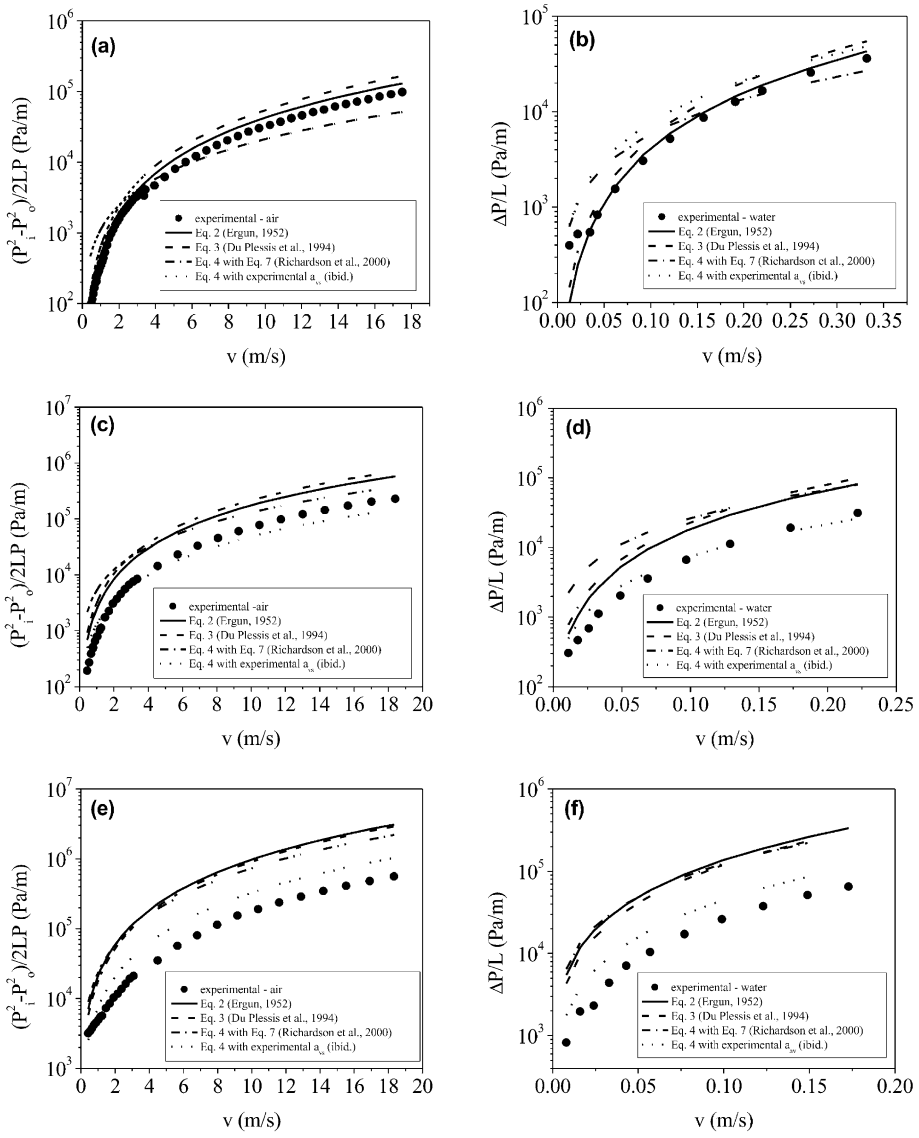


Fig. 9. Comparison between the experimental data and the curves predicted by models from the literature, utilizing the effective porosity, tortuosity and specific surface area, for (a) 8 ppi, air; (b) 8 ppi, water; (c) 20 ppi, air; (d) 20 ppi, water; (e) 45 ppi, air; (f) 45 ppi, water.

Fig. 10 shows the comparison of the measured pressure drop with the one predicted by Eq. (17) for air (Fig. 10a) and water (Fig. 10b) as flowing fluids. It can be seen a very good agreement between measurement and prediction, with small deviations in the whole range of foams and fluids studied, as listed in Table 2. This trend is better visualized in Fig. 11, which compares the values of permeability constants obtained experimentally and those calculated according to the proposed correlation [Equations (18) and (19)]. It is interesting to note that the final correlation showed no direct dependence on the bed tortuosity. This is probably due do the cellular media utilized. The foams are geometrically similar to each other, regardless of their ppi, resulting in a narrow range of $\tau$, as can be seen in Table 1.

## 5. Conclusions

Ceramic foams, obtained from a SiC–$Al_2O_3$ mixture utilizing the replica technique, were tested as filtering medium. Its structure was quantified by measuring the total and effective porosity, tortuosity and specific surface area. These structural parameters were then used to verify the validity of several correlations for permeability prediction, by comparing them with experimental data for air and water flow. No available correlation could predict the pressure drop in the foams for the whole range studied. An Ergun-type empirical correlation, obtained from the data fitting, was proposed.

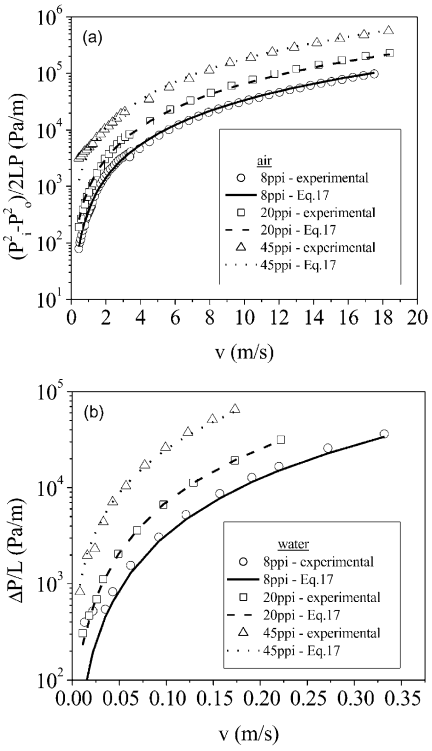


Fig. 10. Comparison between the experimental data and the curves predicted by the proposed Eq. (17), for (a) air and (b) water.

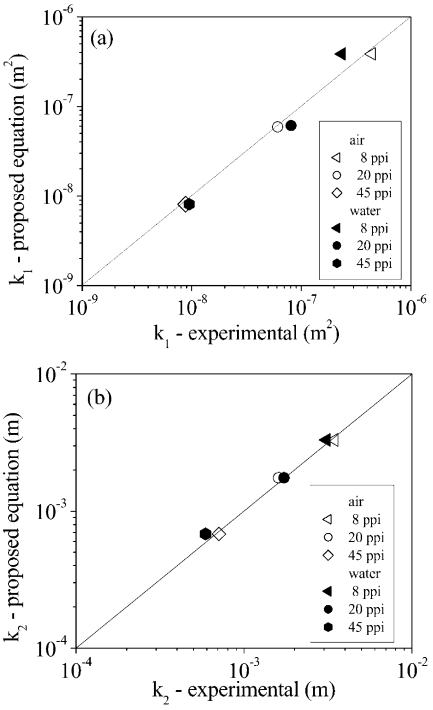


Fig. 11. Comparison of permeability constants obtained experimentally and according to Eqs. (18) and (19). (a) Darcian permeability constant $k_1$; (b) non-Darcian permeability constant $k_2$.

## Acknowledgements

The authors are indebted to FAPESP (proc. 98/15076-0) and to PRONEX-FINEP for the financial support provided. They are also indebted to Dr Vania Salvini and Dr Victor Pandolfelli, from DEMa/UFSCar, for their invaluable help in the ceramic media manufacture, and to Dr. Luis Ruotolo, from DEQ/UFSCar, for the resistivity measurements.

## References

1. Dickenson, C., *Filters and Filtration Handbook, 3rd edn.* Elsevier Science Publishers, Oxford, 1997.
2. Lehtovaara, A. and Mojtahedi, W., Ceramic filters behavior in gasification. *Bioresource Technology*, 1993, **46**, 113–118.
3. Eggersted, P. M., Zievers, J. F. and Zievers, E. C., Choose the right ceramic for filtering hot gases. *Chemical Engineering Progress*, 1993, **January**, 62–68.
4. Acosta, F. A., Castillejos, A. H., Almanza, J. M. and Flores, A., An analysis of liquid flow through ceramic porous media used for molten metal filtration. *Metallurgical and Materials Processing Transactions B*, 1995, **26B**, 159–171.
5. Sheppard, L. M., Porous ceramics: processing and applications. *Ceramic Transactions—Porous Materials, The American Ceramic Society Bulletin*, 1993, **31**, 3–23.
6. Schwarzwalder, K. and Somers, A. V., Method of making porous ceramic articles. *U.S. Patent 3.090.094,* 1963.
7. Innocentini, M. D. M., Gas filtration at high temperatures. PhD. Thesis, Universidade Federal de São Carlos, São Carlos SP, 1997.
8. Richardson, J. T., Peng, Y. and Remue, D., Properties of ceramic foam catalyst supports: pressure drop. *Applied Catalysis A: General*, 2000, **204**, 19–32.
9. Gibson, L. J. and Ashby, M. F., *Cellular Solids—Structure & Properties*. Pergamon Press, Cambridge, 1988.
10. Innocentini, M. D. M., Salvini, V. R., Coury, J. R. and Pandolfelli, V. C., The permeability of ceramic foams. *American Ceramic Society Bulletin*, 1999, **78**(9), 78–84.
11. Ergun, S., Flow through packed columns. *Chemical Engineering Progress*, 1952, **48**(2), 89–94.
12. Macdonald, I. F., El-Sayed, M. S. and Dullien, F. A., Flow through porous media—the Ergun equation revisited. *Industrial and Engineering Chemistry Fundamentals*, 1979, **18**(3), 199–208.
13. Du Plessis, P., Montillet, A., Comiti, J. and Legrand, J., Pressure drop prediction for flow through high porosity metallic foams. *Chemical Engineering Science*, 1994, **49**(21), 3545–3553.
14. Moreira, E. A., Innocentini, M. D. M., Salvini, V. R., Pandolfelli, V. C. and Coury, J. R., Permeability of ceramic foams. *Proceedings of the XXVII ENEMP—Brazilian Congress on Particulate Systems*, 1999, pp. 241–51.
15. Levenspiel, O., *Chemical Reaction Engineering*, 3rd edn. Edgard Blucher Ltda, São Paulo, 2000.
16. Sheidegger, A. E., *The Physics of Flow Through Porous Media*, 3rd edn. Univ. Toronto Press, Toronto, 1974.
17. Montillet, A., Comiti, J. and Legrand, J., Determination of structural parameters of metallic foams from permeametry measurements. *Journal of Materials Science*, 1992, **27**, 4460–4464.
18. Philipse, A. P. and Schram, H. L., Non-Darcian airflow through ceramic foams. *Journal of the American Ceramic Society*, 1991, **74**(4), 728–732.